Supplementary Materials

for

Re-entrance to ferromagnetic insulator with oxygen-vacancy ordering in $La_{0.7}Sr_{0.3}MnO_3/SrTiO_3$ superlattice

Bangmin Zhang,[1,#] Lijun Wu,[2,] Xin Feng,[3] Dongyang Wang,[4] Xiao Chi,[5] Guozhi Chai,[6] Ping Yang,[5] Jun Ding,[3] Jiaguang Han,[4] Jingsheng Chen,[3] Yimei Zhu,[2,*] and Gan Moog Chow[3,*]*

[1]School of Physics, Sun Yat-Sen University, Guangzhou, 510275, China.

[2]Condensed Matter Physics & Materials Science Division, Brookhaven National Laboratory, Upton, New York, 11973, USA.

[3]Department of Materials Science & Engineering, National University of Singapore, 9 Engineering Drive 1, 117576, Singapore.

[4]Center for Terahertz Waves and College of Precision Instrument and Optoelectronics Engineering, Tianjin University and the Key Laboratory of Optoelectronics Information and Technology (Ministry of Education), Tianjin, China.

[5]Singapore Synchrotron Light Source (SSLS), National University of Singapore, 5 Research Link, 117603, Singapore.

[6]Key Laboratory for Magnetism and Magnetic Materials of the Ministry of Education, Lanzhou University, Lanzhou 730000, P. R. China.

*Corresponding authors: ljwu@bnl.gov, zhu@bnl.gov, msecgm@nus.edu.sg

[#]Formerly at Department of Materials Science & Engineering, National University of Singapore, 9 Engineering Drive 1, 117576, Singapore.

Outline

S1: Magnetic properties

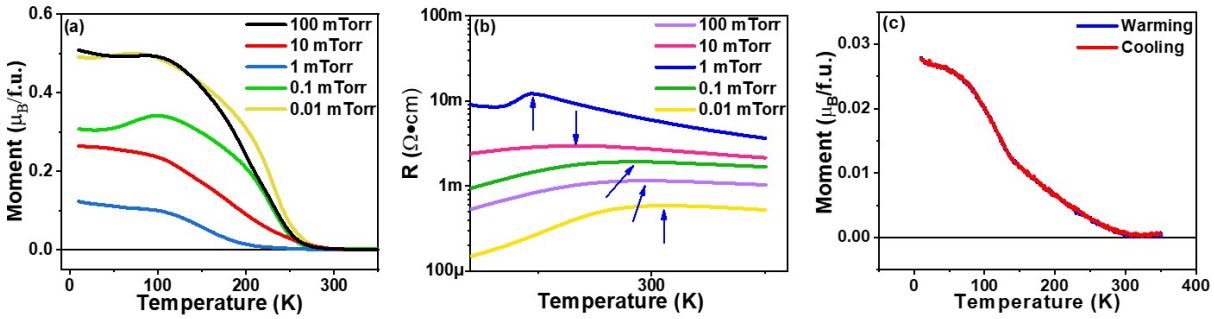

Figure S1: (a) MT curves at in-plane 50 Oe field, and (b) enlarged view of RT curves around insulator-to-metal phase transition for superlattice with different p. "μ_B/f.u." means μ_B per formula unit. The trend of phase transition temperature from MT curve is consistent with that from RT curves. (c) Out-of-plane MT with 50 Oe field for $[LSMO_{10}/STO_5]_5$ superlattice with p = 1 mTorr measured during warming and cooling process.

The MT curves measured at both warming and cooling process shows a kink ~ 129 K, which is different from the transport properties, up-turn of resistivity at 101 K during cooling process and down-turn of resistivity ~ 129 K during warming process. This difference could be understood as below: The phase transition occurs gradually with co-existence of multiphases in manganite. During the cooling process for transport measurement, at the beginning of phase transition the volume of high resistivity phase is low and the low resistivity phase dominates the transport properties without jump ~ 129 K; With further temperature decreases to 101 K, the volume of high resistivity phase increases and dominates the transport properties, which induces the sharp up-turn of resistivity. While for magnetic measurement during cooling process, at the beginning of phase transition ~ 129 K, the magnetic signal of high resistivity phase could be detected even though the volume is not high, and shows the kink in measured out-of-plane MT curve.

S2: Crystal structure

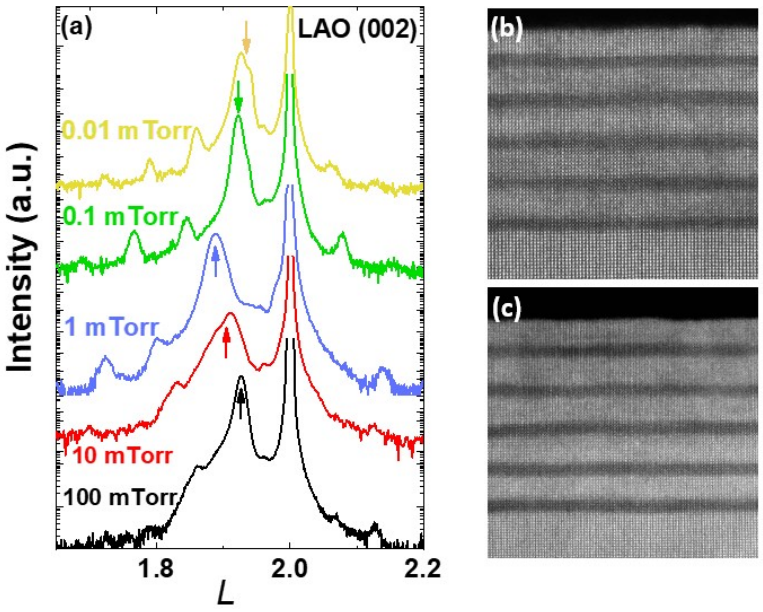

Fig. S2-1: (a) the (002) L scan for $[LSMO_{10}/STO_5]_5$ superlattice; and TEM image for superlattice with p = 100 mTorr (b), and 0.01 mTorr (c). The arrows show the superlattice (002) peak. These results show the formation of superlattice configuration.

The crystal structure, including the lattice constant and MnO_6 octahedral rotation, has been measured for superlattice under different oxygen pressure p. The L scan around (002) peak was shown in Fig. S2-1. The superlattice with p = 1 mTorr shows a good (002) peak with satellites due to the scattering between LSMO/STO interfaces, which indicates good quality of LSMO/STO interface and good coherence between them. For superlattice with other p, signal of strain relaxation occurs according to the (-103) RSM with $\boldsymbol{H}$ deviating from -1 in Fig.S2-2, however, the satellites due to the scattering between LSMO/STO interface still appears with relatively low intensity. These results reveal that the multilayer with different p indeed forms the superlattice configuration, which is supported by the TEM results above. However, these superlattices are not perfect due to the strain relaxation and/or the diffusion of oxygen vacancy. For example, the satellites due to the scattering between the LSMO/STO surface and

superlattice/substrate interface, is missing, revealing reduced coherence between these two interfaces with large total thickness.

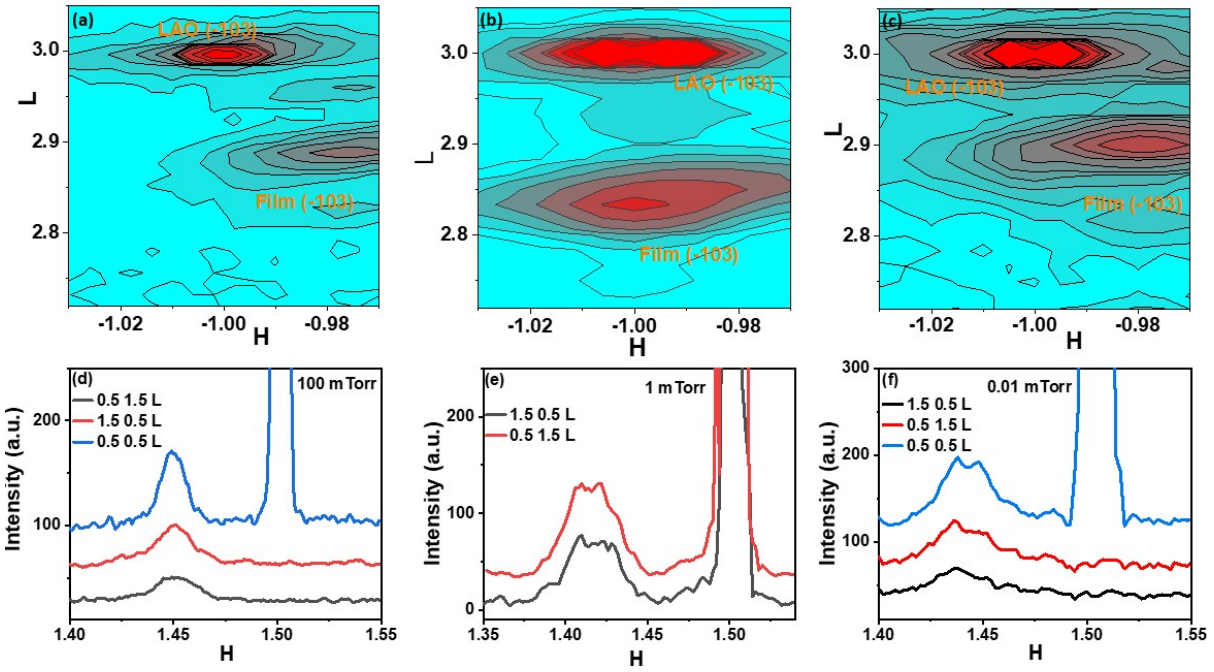

Fig. S2-2: (a-c) the (-103) RSM, and (d-f) half-integer diffraction for $[LSMO_{10}/STO_5]_5$ superlattice with p = 100 mTorr, 1 mTorr, and 0.01 mTorr, respectively. The trend of lattice constant and oxygen octahedral rotation with oxygen pressure is summarized in the inset of Fig. 1d.

The MnO_6 octahedral rotation pattern from half-integer diffraction is $a^0a^0c^-$ for p = 1 mTorr, and with the deviation of oxygen pressure from 1 mTorr (either decreasing or increase oxygen pressure), the MnO_6 octahedral rotation pattern gradually changes into $a^-a^-c^-$. Previous simulation on oxide in perovskite structure has shown that with the oxygen vacancy locating on the AO plane of ABO_3 structure, the $a^0a^0c^-$ rotation is stabilized, consistent with current experimental observations. The crystal structure of superlattice at different pressure should result from the structural optimization with corresponding chemical environment. The out-of-plane lattice of superlattice with p = 1 mTorr is largest with lowest in-plane lattice constant, which is clamped by the substrate. The enhanced tetragonal distortion with c/a > 1 in superlattice with p = 1 mTorr would lower the energy position of $3d_{z^2-r^2}$ orbital, preferred for

electron occupancy. The introducing of oxygen vacancy by diffusion from STO, donating two electrons to the LSMO unit cell, tends to increase the Mn out-of-plane $3d_{z^2-r^2}$ orbitals occupancy first, as revealed in the polarization dependent O *K* edge XAS. For superlattice with p = 1 mTorr, the major signal in reciprocal space mapping (RSM) shows no strain relaxation. The width along *L* direction of signal from superlattice in (-103) RSM is relatively wide, which is related to the LAO substrate (-103) RSM with wide width along *L* direction. After careful examination, the signal with strain relaxation is weak, which would disturb the ordering of oxygen vacancy on (001) La/SrO-plane. However, due to the relative weak intensity of strain relaxation, the overall properties should be determined by the fully-strained part of superlattice. For superlattice with other p, the oxygen vacancy would distribute on both (001) La/SrO plane and (001) MnO_2 plane, which tend to enlarge both the in-plane and out-of-plane lattice constant. Then the strain relaxation occurs with enlarged in-plane lattice constant and decreased out-of-plane lattice constant, compared to that of p = 1 mTorr. The tetragonal distortion become weak and then the anisotropy of electron occupancy decreases.

S3: Transport properties

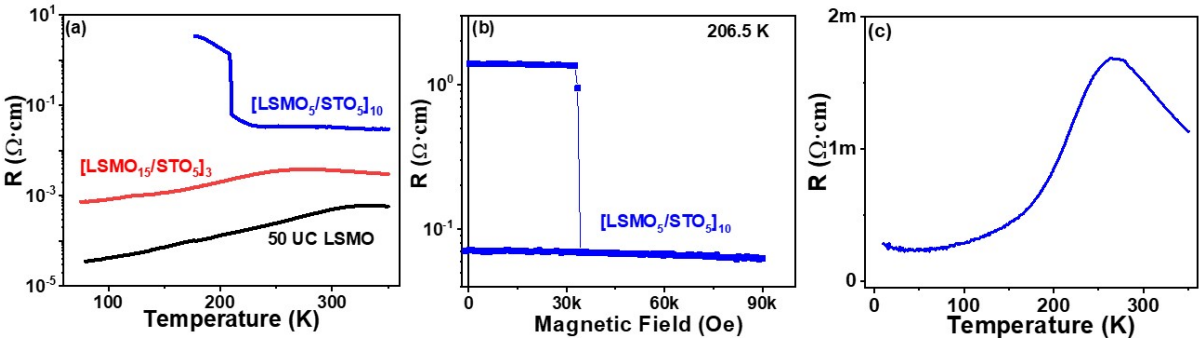

Figure S3: (a) RT without magnetic field measured during warming process for different superlattices; (b) MR at 206.5 K for $[LSMO_5/STO_5]_{10}$ superlattice. Before measurement, it was cooled down to 100 K and then warmed up to the setpoint. (c) the RT of $[LSMO_{10}/STO_5]_5$ superlattice with p = 1 mTorr after 1-hour post annealing under atmosphere at 800 °C.

$[LSMO_5/STO_5]_{10}$, $[LSMO_{15}/STO_5]_3$ superlattice and 50 UC single LSMO layer, have been fabricated on (001) LAO substrate with p = 1 mTorr during STO growth. All LSMO layer was grown at 100 mTorr. For the 50 UC LSMO single layer, it was annealed at 1 mTorr for 55 seconds (time required to grow 5 UC STO under 1 mTorr) after every 10 UC LSMO growth, and then grow next 10 UC LSMO at 100 mTorr. Only the $[LSMO_5/STO_5]_{10}$ shows the sudden jump of resistivity in RT ($\boldsymbol{T}_O$ = 209 K) and MR (H = 34 kOe at 206.5 K) curves, indicating the existence of CDW.

Both the STO/LSMO interface and the central part of LSMO layer affects the transport properties. With the increase of LSMO thickness in one period of superlattice, the temperature point of high resistivity CDW phase with abrupt jump decrease: $\boldsymbol{T}_O$ = 209 K for SL with 5 UC LSMO in one period, $\boldsymbol{T}_O$ = 128 K for SL with 10 UC LSMO in one period, and no $\boldsymbol{T}_O$ for SL with 15 UC LSMO in one period. Below $\boldsymbol{T}_O$, it is high resistivity CDW phase. With increase of LSMO thickness, the temperature range with CDW feature decrease. This trend could be understood as below: A part of the LSMO layer close to the STO/LSMO interface is affected by the interface (defined as interfacial region), and the left region around the central part of

LSMO layer is unaffected by the STO/LSMO interface which should present different properties from that of interfacial region. With the same extent of LSMO range (interfacial region) affected by each STO/LSMO interface, the superlattice with larger LSMO thickness in each period should have larger unaffected region, and the total transport properties should show more feature of unaffected region. While in current work, the feature of high resistivity CDW phase decrease with increasing LSMO thickness in one period of superlattice, which should not come from the central part of LSMO layer. Hence, the affected interfacial region should be responsible for the formation of CO/CDW.

S4: O K edge & Mn L edge EELS

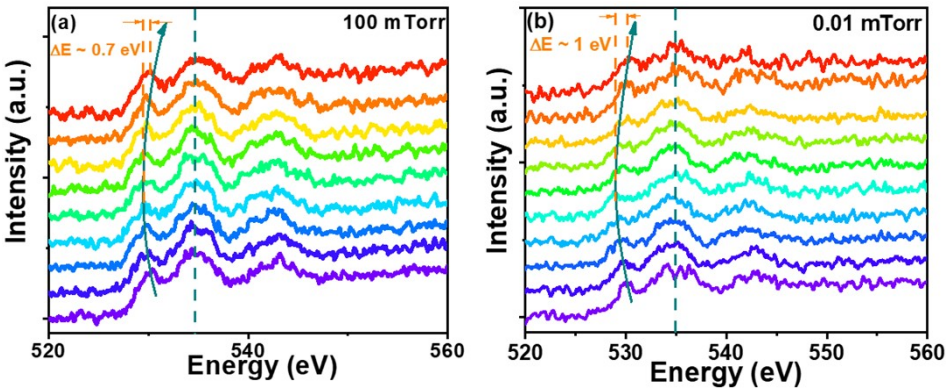

Figure S4-1: the unit-cell resolved O K edge EELS of LSMO layer for $[LSMO_{10}/STO_5]_5$ superlattice with (a) p = 100 mTorr and (b) p = 0.01 mTorr. Along the arrow direction, it goes from bottom interface to the top interface across one LSMO layer.

Unit cell-resolved O K edge EELS of LSMO layer for superlattice with different with p = 100 mTorr and 0.01 mTorr are shown above. Same as that in superlattice with p = 1 mTorr, Mn chemical valence increase from the LSMO/STO interface to the center of LSMO layer. The energy difference between pre-edge and main peak ΔE is ~ 0.7 eV and ~ 1 eV for p = 100 mTorr and 0.01 mTorr, respectively, which is larger than that with p = 1 mTorr. See text for discussion on the trend of ΔE with oxygen pressure.

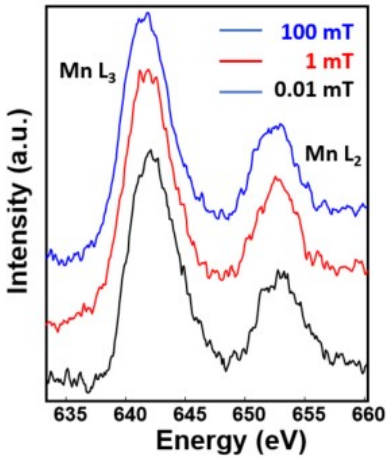

Figure S4-2: The averaged Mn K edge EELS of LSMO layer for different pressure p. The difference of peak position is not enough to identify the chemical valence. See text for more discussion.

S5: EELS

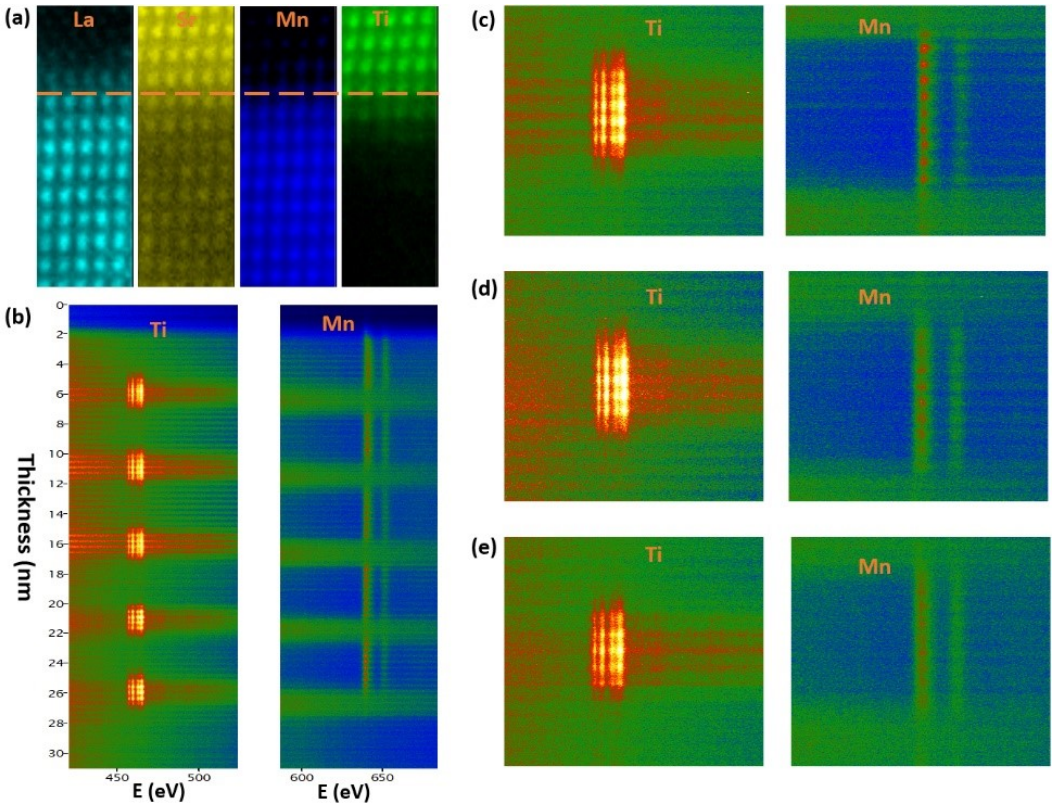

Figure S5-1: (a) The illustration of atomic-resolved 2D EELS image around LSMO/STO interface and (b) the layer resolved EELS for whole superlattice with oxygen pressure p = 1 mTorr; the enlarged view of STO layer (left) and LSMO layer (right) for superlattice with oxygen pressure at (c) 100 mTorr; (d) 1 mTorr and (e) 0.01 mTorr, respectively.

Based on atomic 2D EELS image in Fig. S5-1(a), all cations, including La, Ti and Mn, shows ionic diffusion with extent of 1-2 unit cells. In order to get more information, the atomic layer-resolved Ti and Mn EELS signal of whole superlattice fabricated at different pressure was shown in Fig. S5-1(b)-(e). Detailed analysis shows the 1D plot of the maximum intensity of Ti (peak ~ 465 eV in Fig. 2a) and Mn (peak ~ 642 eV in Fig. S4-2) EELS for different superlattices in Fig. S5-2. With different p, the cationic interdiffusion shows similar trend with the extent of ~ 2 unit cells, consistent with the 2D EELS image. Cation mixing occurs at the interface for all superlattice, however, the range of cationic diffusion does not show obvious dependence on the oxygen pressure p during STO growth. Previous work reveals that the

interdiffusion has close relationship with the interfacial conditions around hetero-structural interface, and depends on the background gas pressure. In current work, the high oxygen pressure 100 mTorr during LSMO growth might affect the length of cationic interdiffusion.

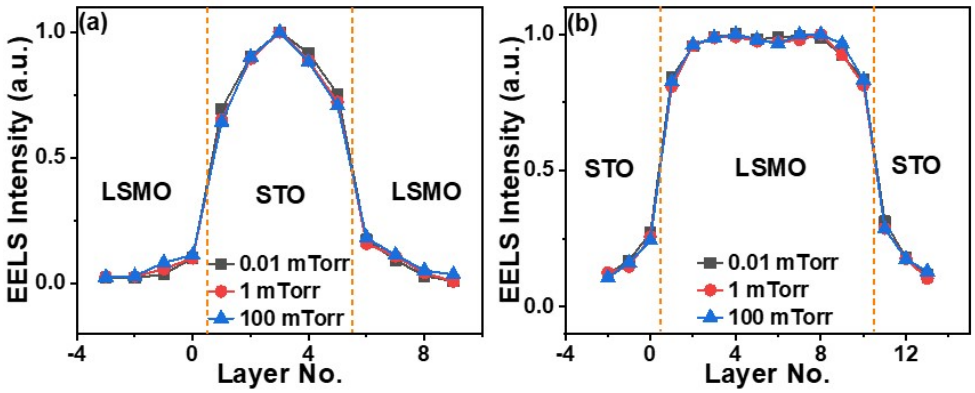

Figure S5-2: the 1D plot of the maximum intensity of (a) Ti and (b) Mn L edge EELS for $[LSMO_{10}/STO_5]_5$ superlattice with different p. The profile was normalized for comparison between different superlattices. The orange dashed line indicates the LSMO/STO interface.

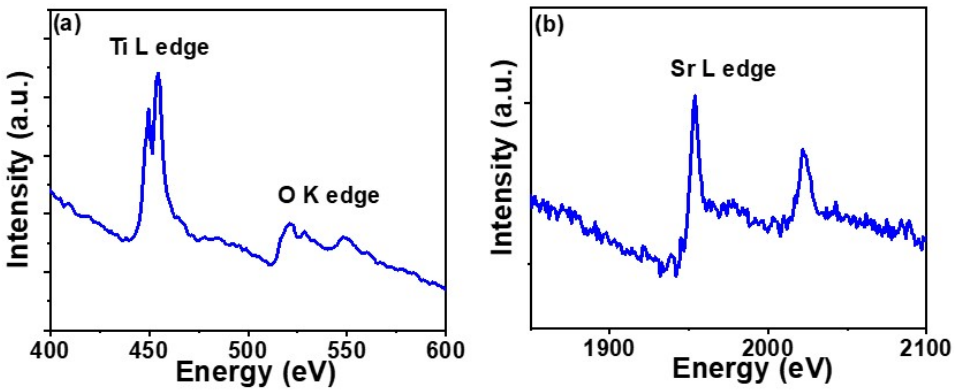

Figure S5-3: (a) The Ti and (b) Sr L edge EELS curve for $[LSMO_{10}/STO_5]_5$ superlattice with p = 1 mTorr for atomic ratio evaluation. The Sr/Ti ratio was evaluated using the standard tool in Gatan Microscopy Suite Software.

Around the heterostructural interface, the cationic stoichiometry, defects, cationic inter-mixing, and materials properties depends on the fabrication parameters, especially the cationic composition of the $SrTiO_3$. The Sr/Ti ratio of $SrTiO_3$ was evaluated based on averaged EELS curve as shown in Fig. S5-3 using the standard tool in Gatan Microscopy Suite Software. The averaged Sr/Ti ratio of whole STO layer (5 UC) for p = 0.01 mTorr, 1 mTorr and 100 mTorr,

are 0.96, 0.98, 1.03, respectively. Previous work (*Journal of Physics D: Applied Physics* 2014, 47(3), 034009) indicates that the background gas tend to scatter the lighter ions (Ti), which causes Sr/Ti ratio > 1 in film with $\boldsymbol{J}$ = 1 J/cm^2, and stoichiometric Sr/Ti ~ 1 with $\boldsymbol{J}$ ~ 1.4 J/cm^2 under oxygen pressure ~ 10 mTorr. With the increase of background oxygen pressure, the scattering of Ti tends to increase. In current work, the high Sr/Ti ratio with 100 mTorr should come from the strong scattering of Ti by background gas; with decrease of background pressure, Sr/Ti ratio decrease with less scattering effect from background gas. Although the uncertainty of estimated Sr/Ti ratio exists, the trend of Sr/Ti ratio with oxygen pressure *p* should be valid. The Sr/Ti ratio normally shows monotonous trend with oxygen pressure with fixed laser fluence, while both the magnetic and transport of superlattice with oxygen pressures *p* shows non-monotonous behavior, which imply that the transport properties are not dominated by the Sr/Ti ratio with changing oxygen pressure.

S6: Polarization-dependent X-ray absorption

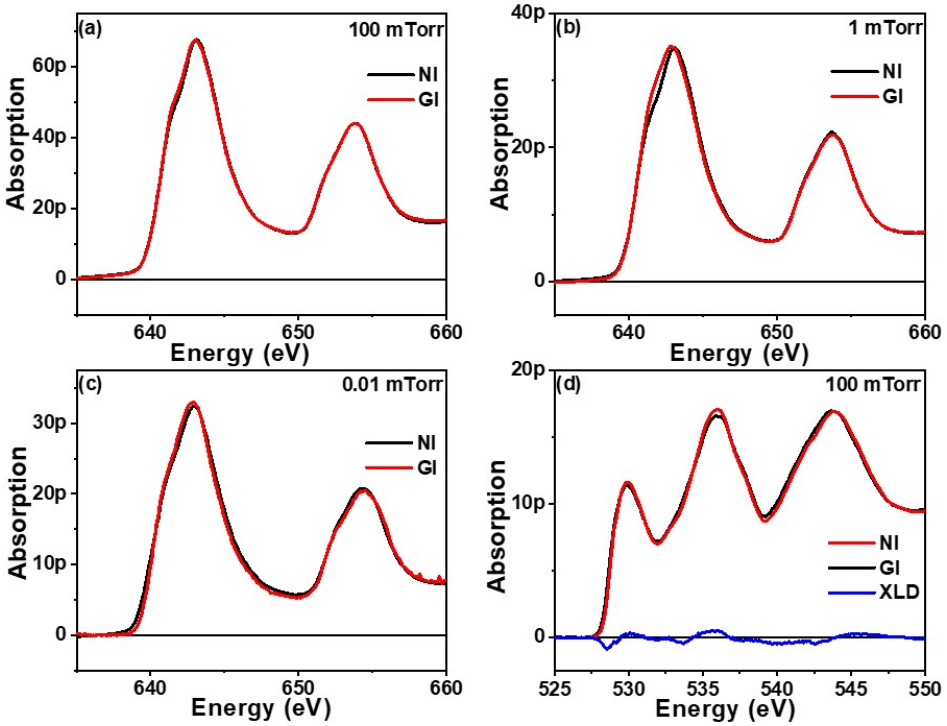

Figure S6: Polarization-dependent Mn *L* edge for superlattice with oxygen pressure at (a) 100 mTorr; (b) 1 mTorr and (c) 0.01 mTorr, respectively; (d) Polarization-dependent O *K* edge XAS with p = 100 mTorr.

S7: Magnetoresistance

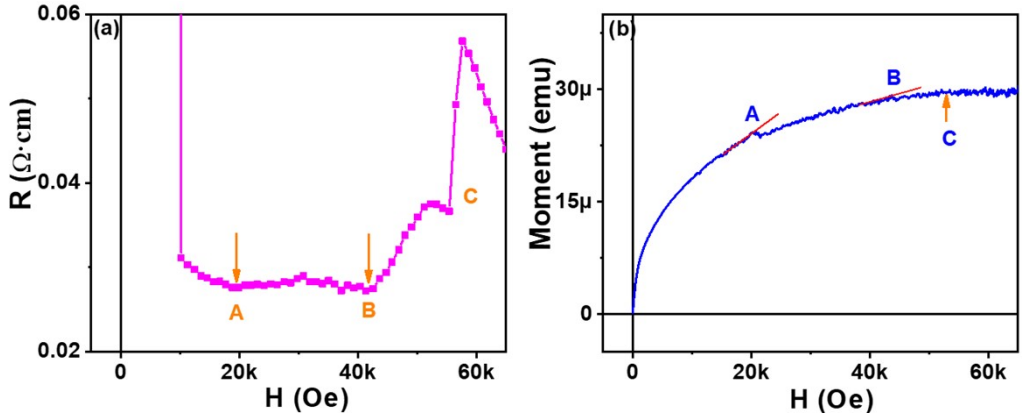

Fig. S7-1: The enlarged view of (a) MR and (b) out-of-plane MH at 120 K for $[LSMO_{10}/STO_5]_5$ superlattice with p = 1 mTorr. The accuracy of the SQUID for MH loop is in the order of 1E-7 emu, and the jump around point A and B is not due to the measurement error.

At $\boldsymbol{T}$ = 120 K, the resistivity increases with increasing $\boldsymbol{H}$ at A (2.1 T), B (4.3 T), and C (5.1 T), as enlarged in Fig. S7-1. The out-of-plane magnetic curve shows a sudden change around A and B, suggesting the change of magnetization structure. Then the increase of resistivity at A and B should come from the fluctuation of the magnetic domain structure. However, there is no obvious magnetism change around C in MH curve, and the origin was discussed in the main text.

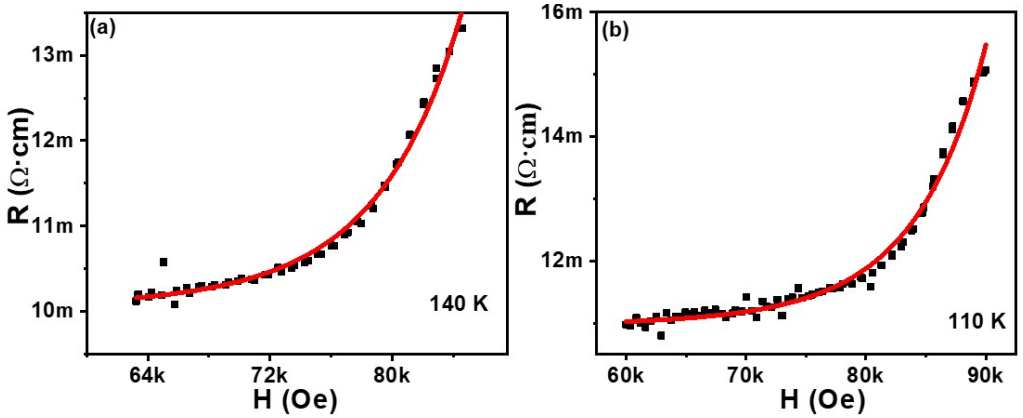

Fig. S7-2: MR for $[LSMO_{10}/STO_5]_5$ superlattice with p = 1 mTorr at different temperatures. The red curve is the fitted line with VRH model. See text for discussion.